Electronic Supplementary Information

Three-dimensional porous copper-decorated bismuth-based nanofoam for boosting electrochemical reduction of CO_2 to formate

Yingchun Zhang,[a,b] Changsheng Cao,[a,b,*] Xin-Tao Wu[a,b,c] and Qi-Long Zhu[a,b,c,*]

[a] State Key Laboratory of Structural Chemistry, Fujian Institute of Research on the Structure of Matter, Chinese Academy of Sciences (CAS), Fuzhou 350002, China

[b] University of Chinese Academy of Sciences, Beijing 100049, China

[c] Fujian Science & Technology Innovation Laboratory for Optoelectronic Information of China, Fuzhou 350108, China

*Corresponding Author E-mail: cscao@fjirsm.ac.cn, qlzhu@fjirsm.ac.cn

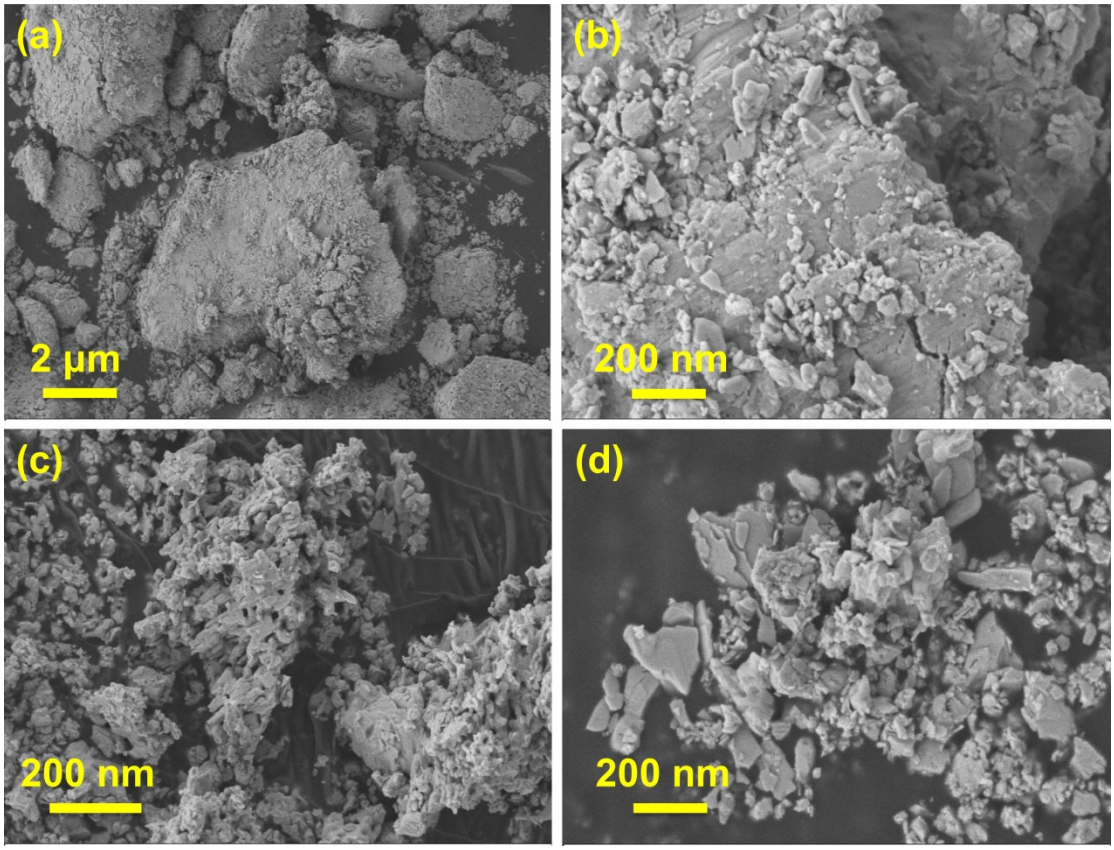

Fig. S1 SEM images of (a, b) commercial bulk Bi and (c, d) P-Bi.

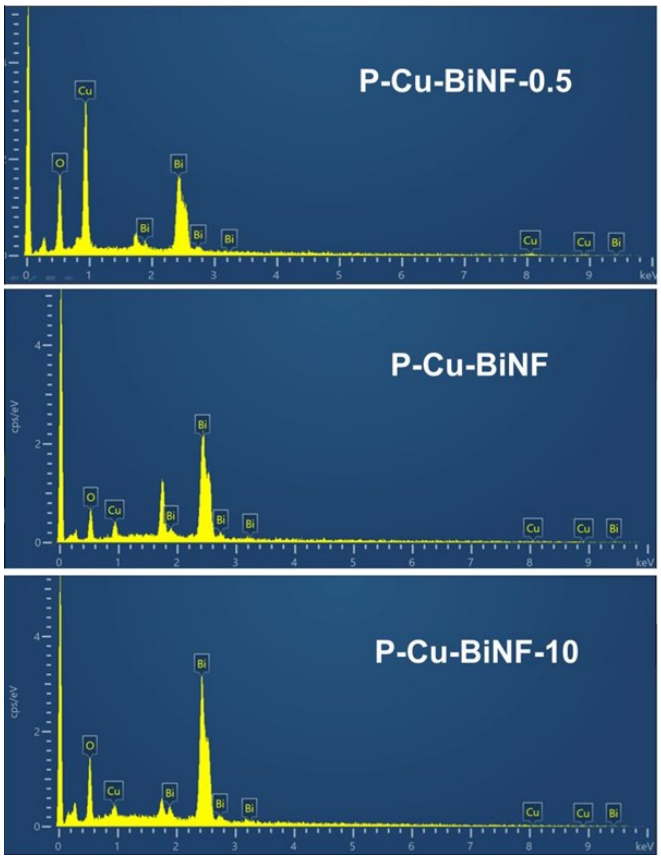

P-Cu-BiNF-0.5

Element	Atomic percent (%)
Bi	15.89
Cu	35.16
O	48.95

P-Cu-BiNF

Element	Atomic percent (%)
Bi	41.43
Cu	8.94
O	49.63

P-Cu-BiNF-10

Element	Atomic percent (%)
Bi	34.24
Cu	3.70
O	62.06

Fig. S2 SEM-EDX images of P-Cu-BiNF-0.5, P-Cu-BiNF and P-Cu-BiNF-10.

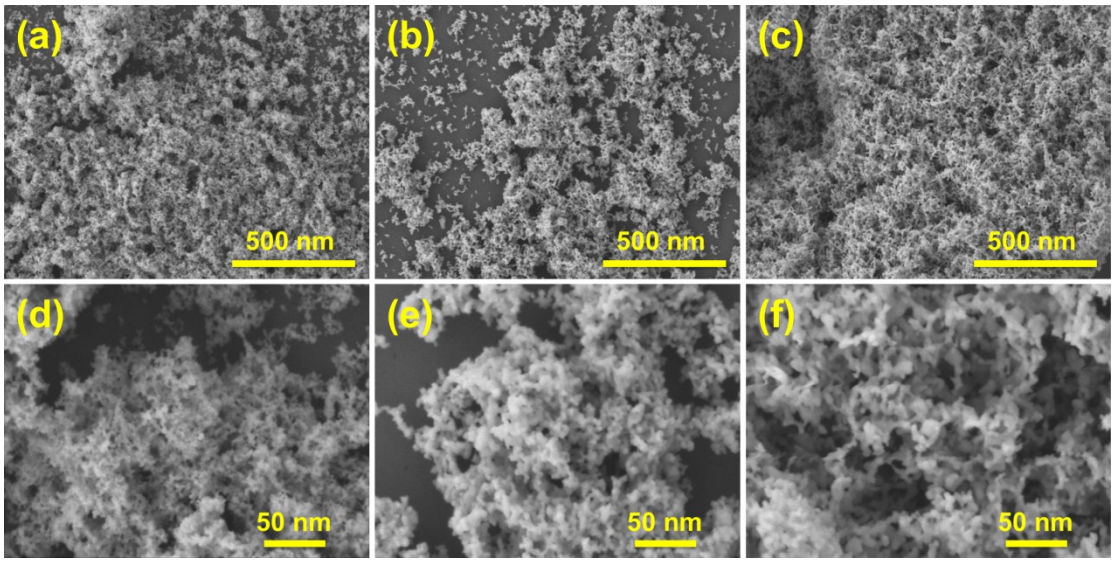

Fig. S3 SEM images of (a, d) P-Cu-BiNF-0.5, (b, e) P-Cu-BiNF and (c, f) P-Cu-BiNF-10.

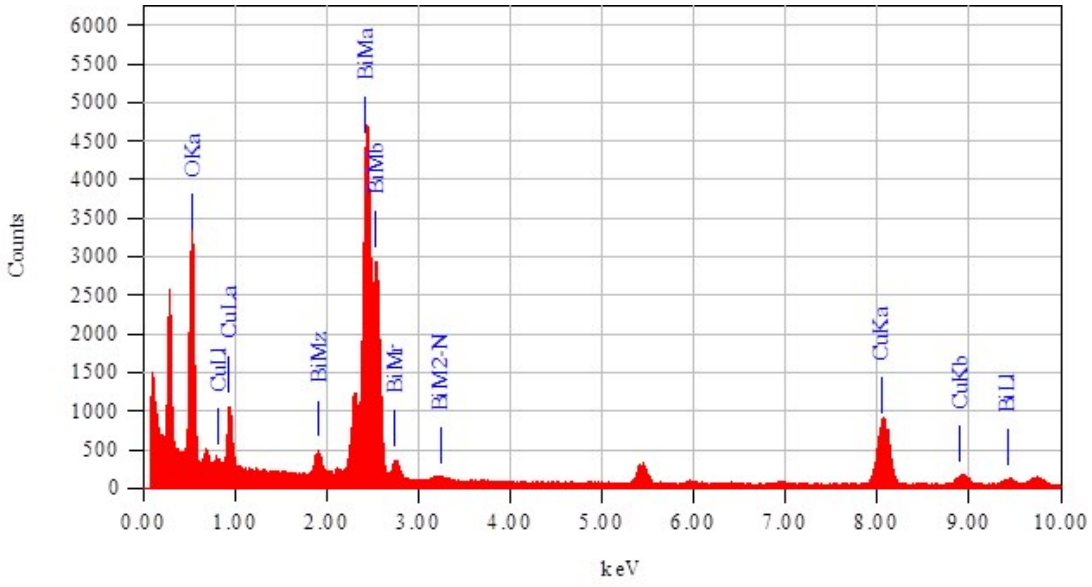

Element	Atom%	Atom%	Atom%	Average atom%
Bi	27.06	30.47	27.37	28.30
Cu	12.21	12.62	12.26	12.36
O	60.73	56.91	60.38	59.34

Fig. S4 TEM-EDX images of P-Cu-BiNF.

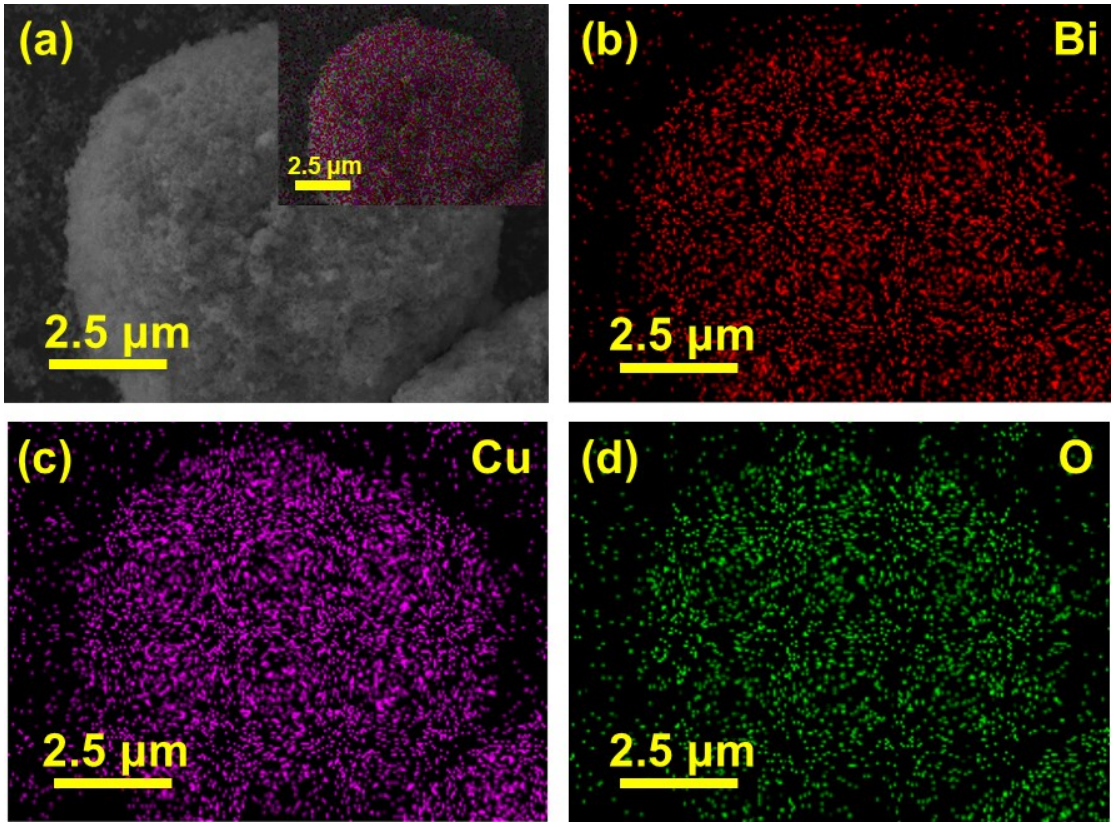

Fig. S5 SEM-Mapping images of P-Cu-BiNF-0.5.

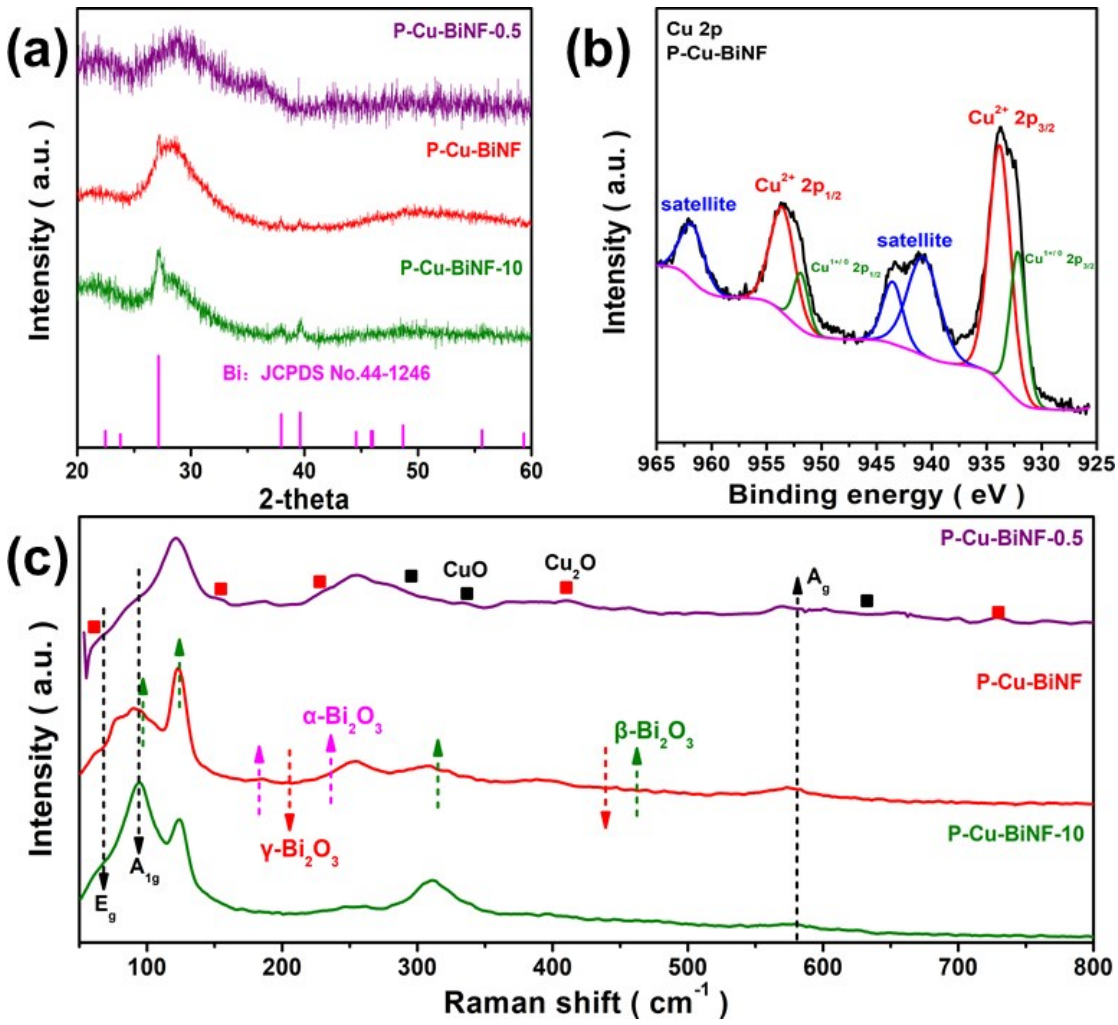

Fig. S6 (a) PXRD patterns. (b) XPS Cu 2p spectra of P-Cu-BiNF. (c) Raman spectra of P-Cu-BiNF-0.5, P-Cu-BiNF and P-Cu-BiNF-10 (the arrows represent Bi and Bi_2O_3 phases, and the squares represent Cu_2O and CuO phases).

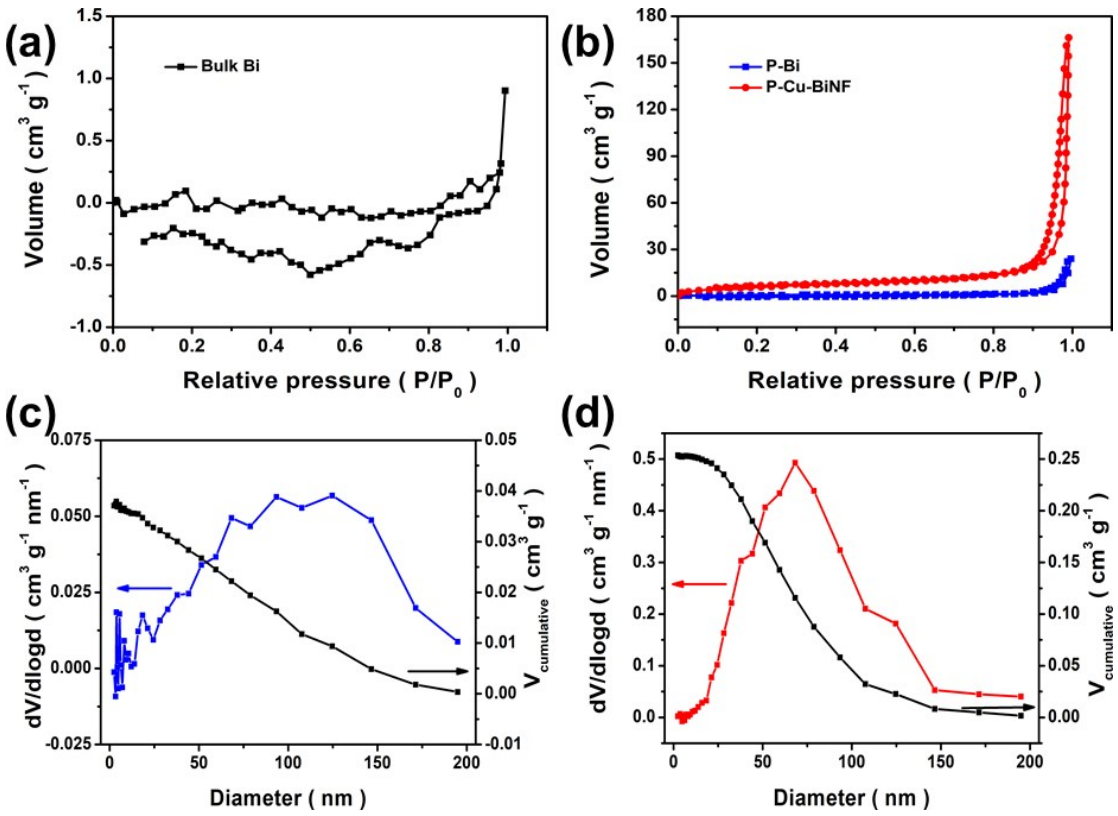

Fig. S7 (a) N_2 sorption isotherm for bulk Bi. (b) N_2 sorption isotherm for P-Bi and P-Cu-BiNF. Pore size distributions and cumulative pore volumes ($V_{vumulative}$) of (c) P-Bi and (d) P-Cu-BiNF.

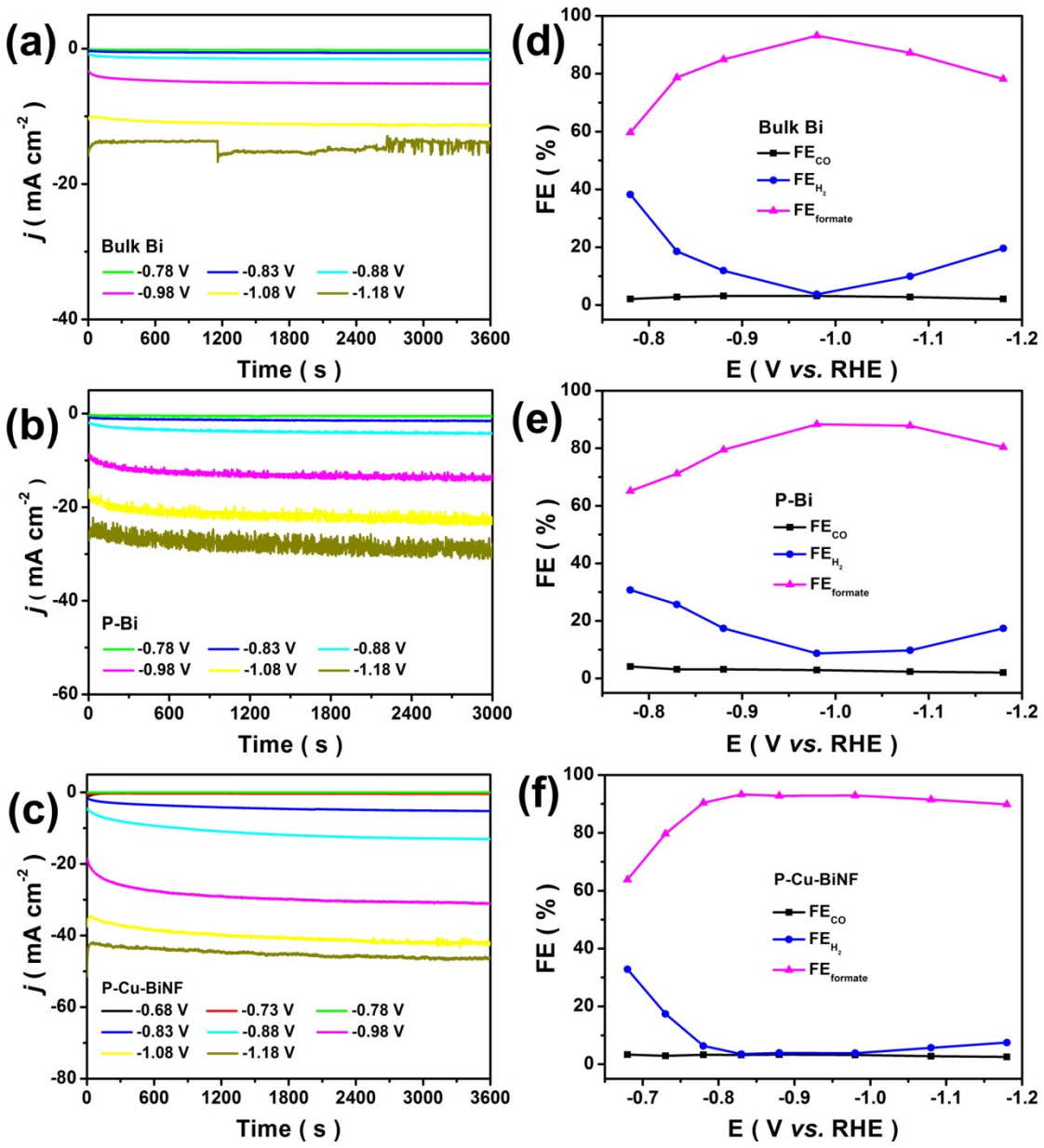

Fig. S8 Potential-dependent i-t curves and FEs of H_2, CO and formate for (a, d) bulk Bi, (b, e) P -Bi and (c, f) P-Cu-BiNF.

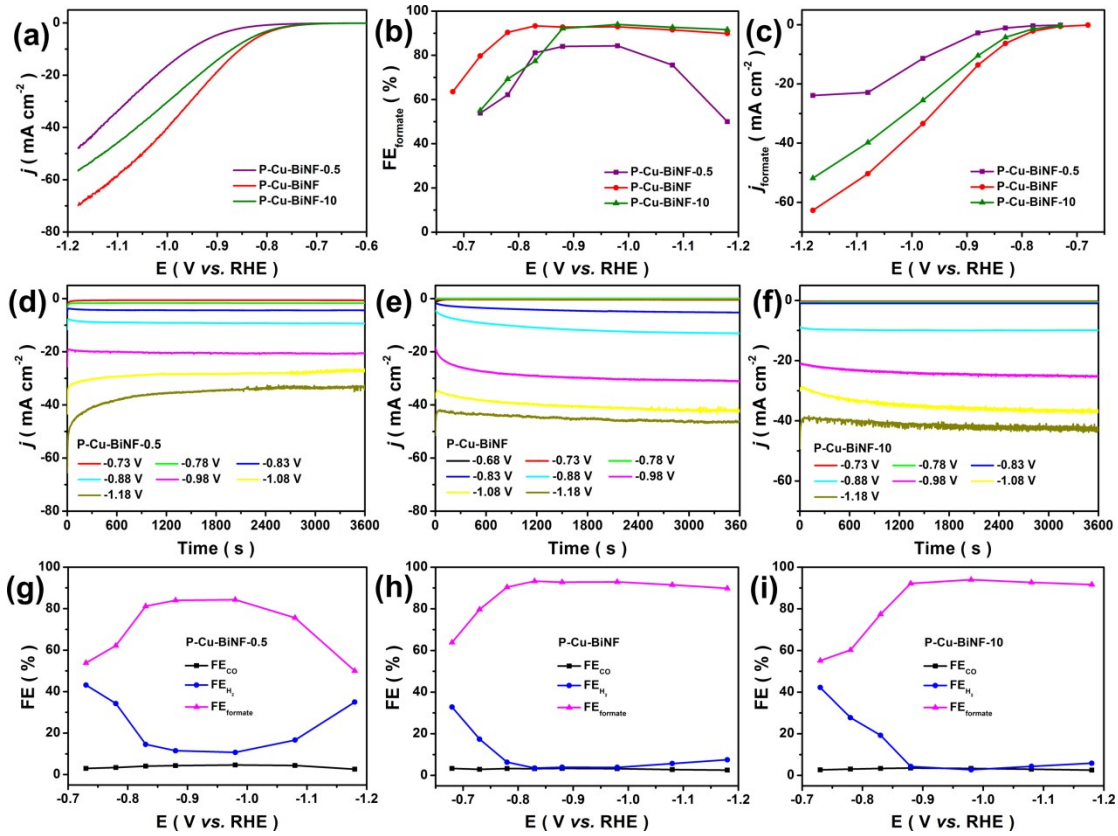

Fig. S9 (a) LSV curves, (b) $FE_{formate}$ and (c) $j_{formate}$ for P-Cu-BiNF-0.5, P-Cu-BiNF and P-Cu-BiNF-10; Potential-dependent i-t curves and FEs of H_2, CO and formate for (d, g) P-Cu-BiNF-0.5, (e, h) P-Cu-BiNF and (f, i) P-Cu-BiNF-10.

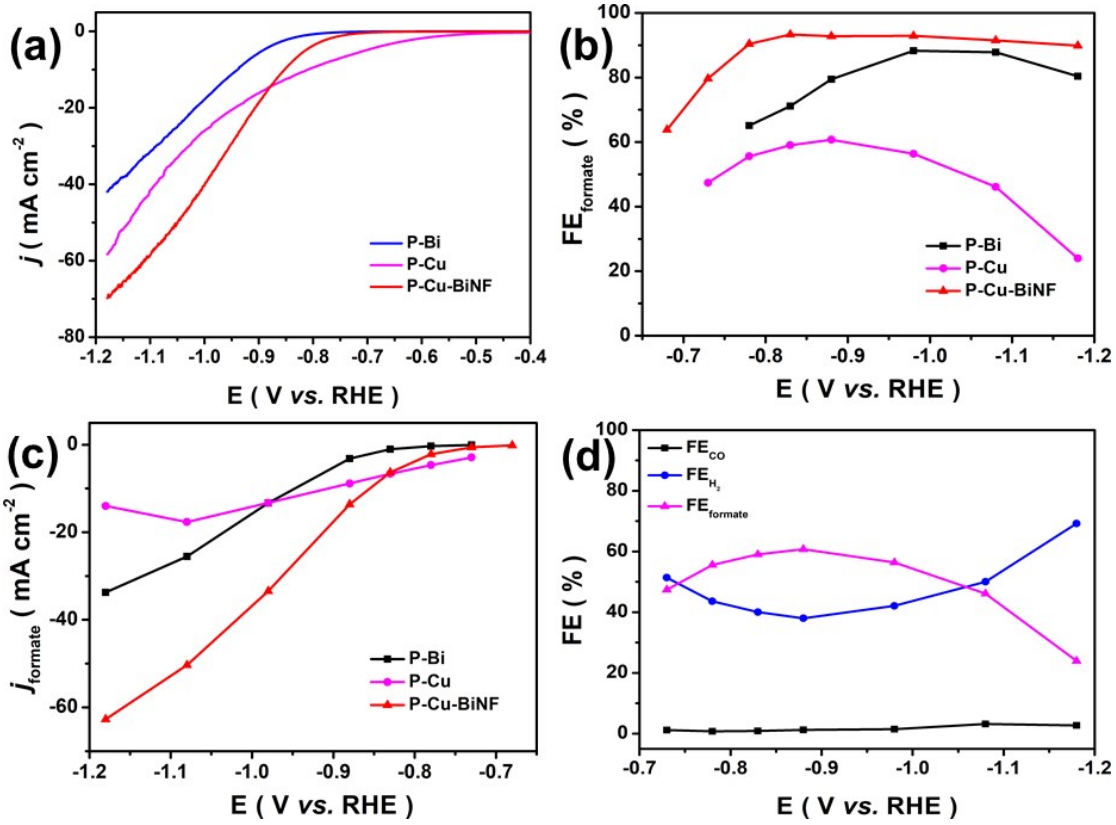

Fig. S10 (a) LSV curves, (b) $FE_{formate}$ and (c) $j_{formate}$ for P- Bi, P-Cu and P-Cu-BiNF, (d) FEs of H_2, CO and formate for P-Cu.

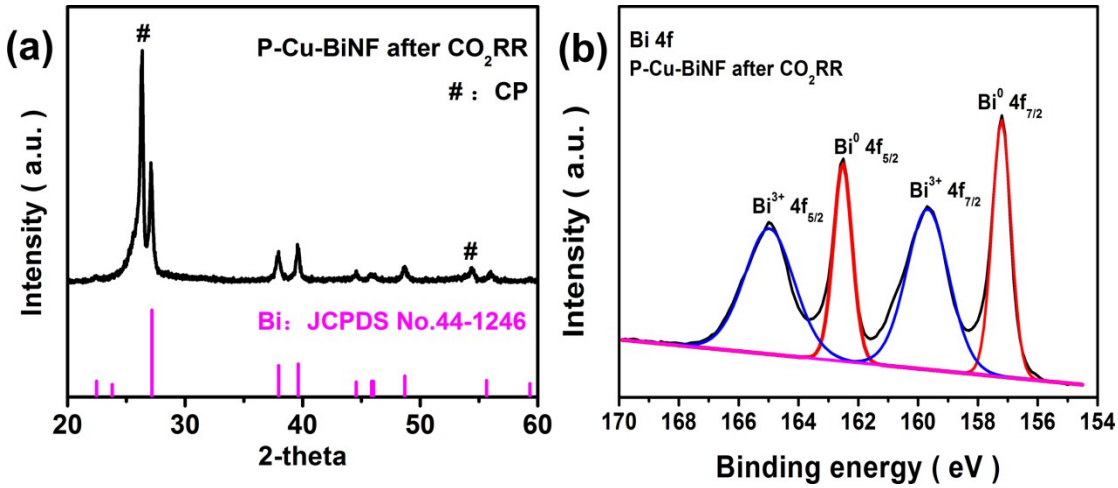

Fig. S11 (a) PXRD pattern and (b) Bi 4f XPS spectrum of P-Cu-BiNF after CO_2RR. (CP represents carbon paper).

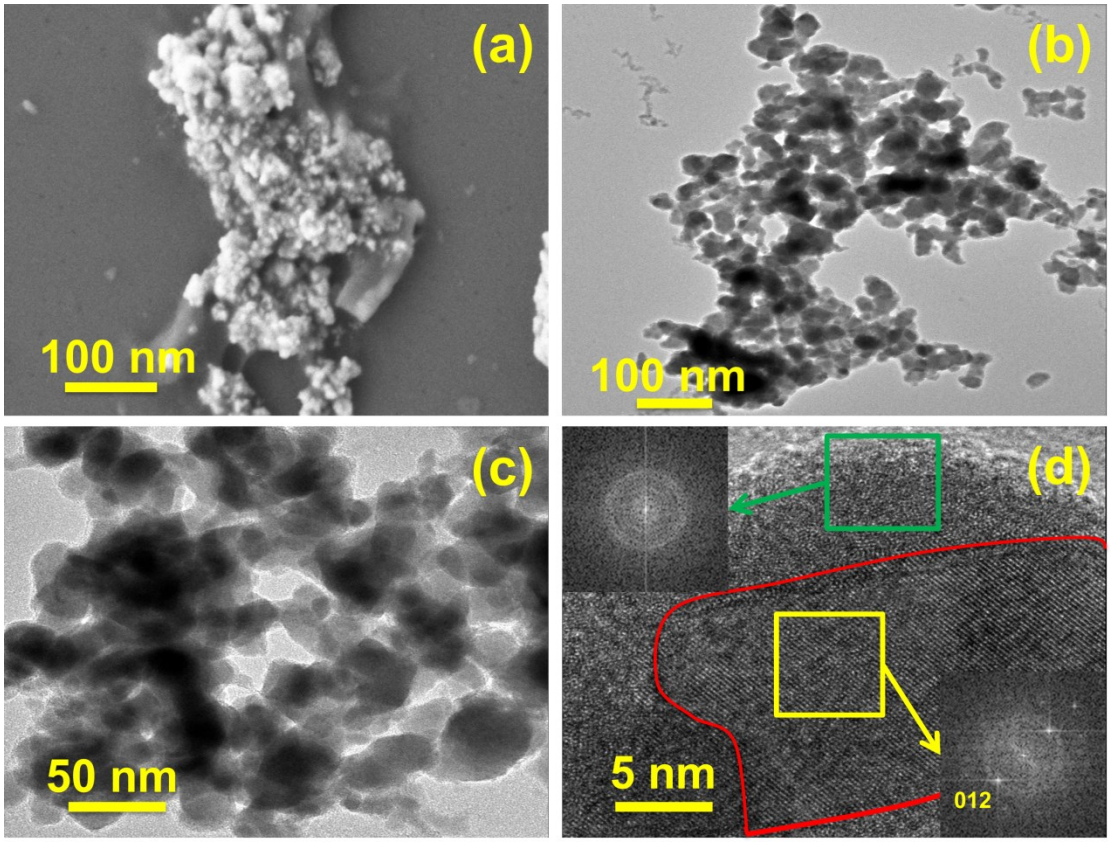

Fig. S12 (a) SEM, (b-c) TEM and (d) HRTEM images of P-Cu-BiNF after CO_2RR.

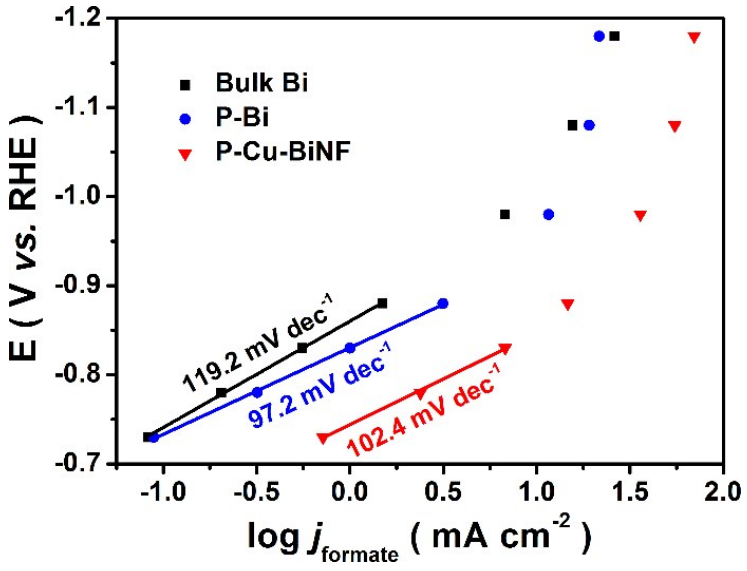

Fig. S13 Tafel plots of P-Cu-BiNF, P-Bi and bulk Bi.

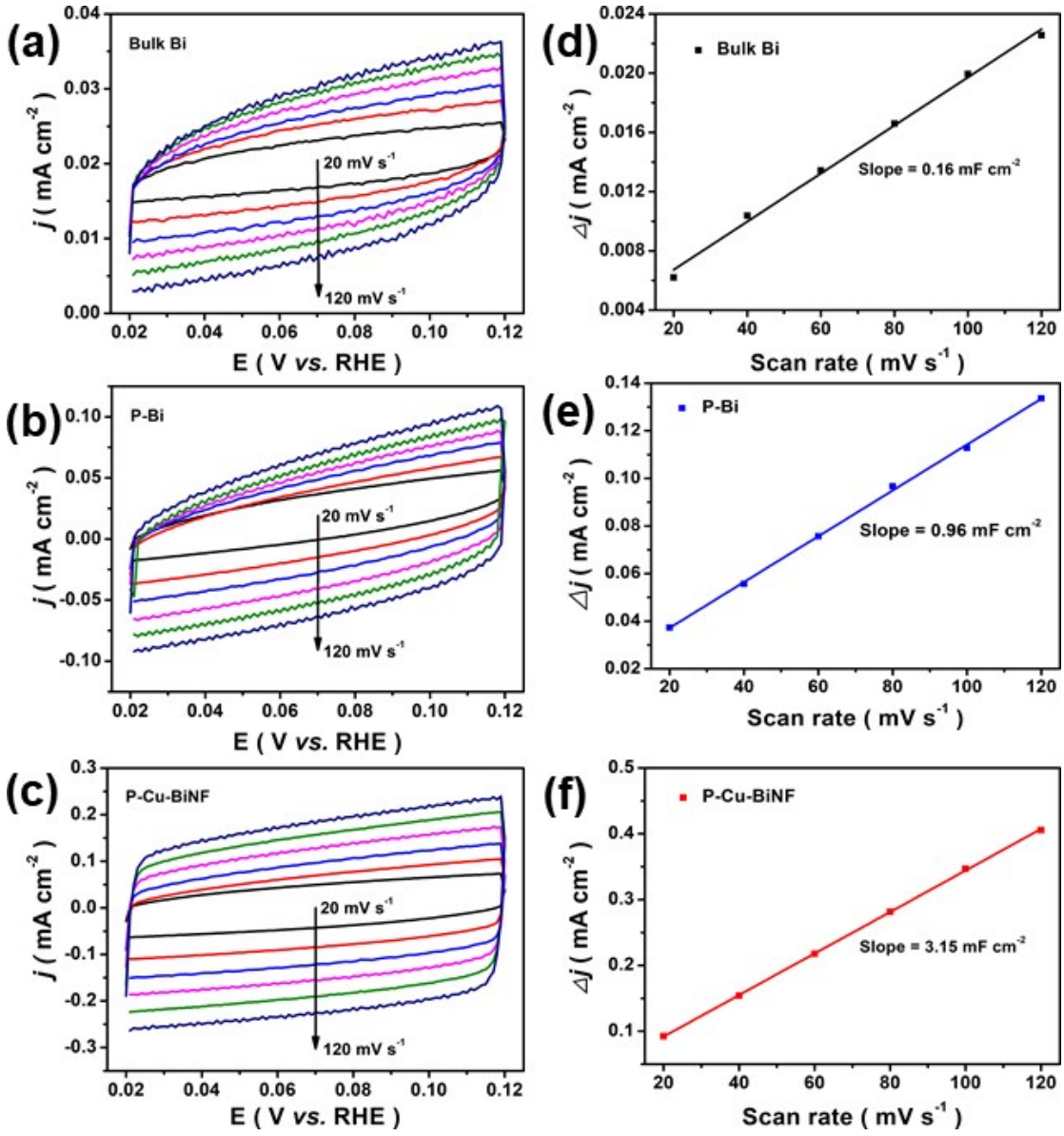

Fig. S14 CV curves at different scan rates and Δj ($= j_a - j_c$) against scan rates for (a, d) bulk Bi, (b, e) P -Bi and (c, f) P-Cu-BiNF.

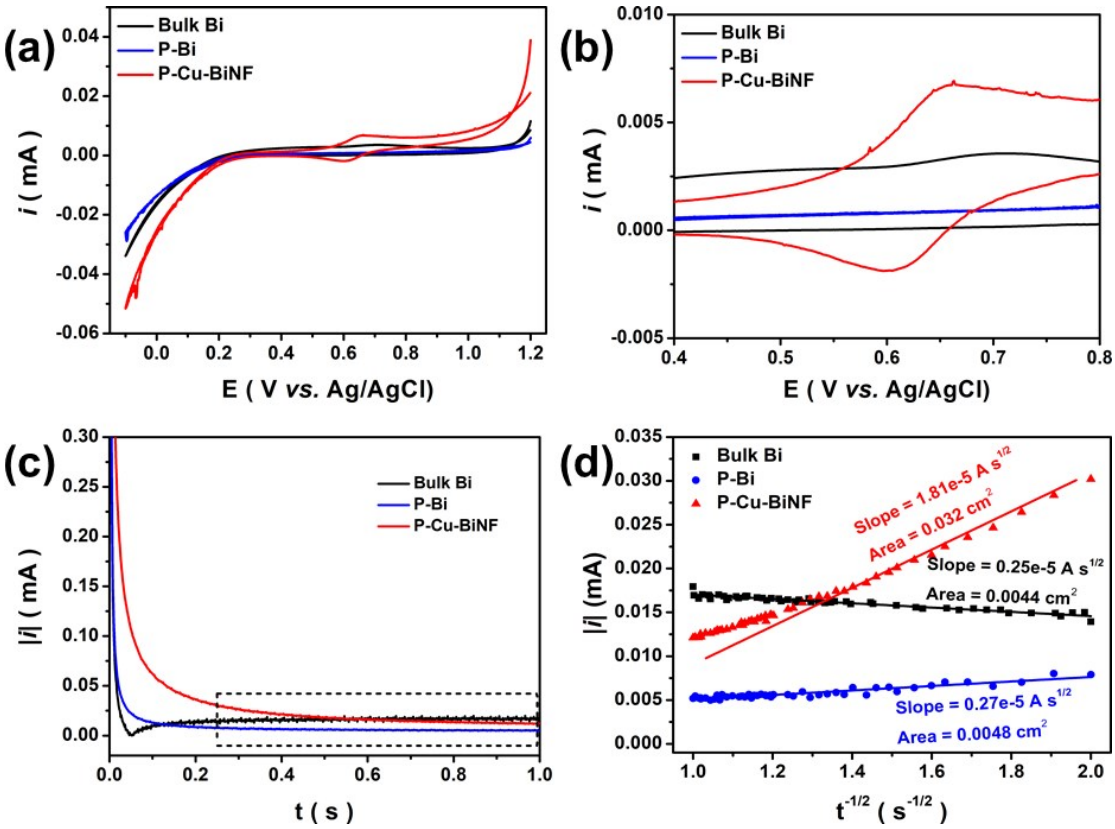

Figure S15 (a) CV curves at the sweep rate of 5 mV s^{-1} in 0.1 M KCl (containing 5 mM $K_3Fe(CN)_6$) over bulk Bi, P-Bi and P-Cu-BiNF. (b) The magnified of (a). (c) Chronoamperometric response recorded in 0.1 M KCl (containing 5 mM $K_3Fe(CN)_6$) after stepping the potential from 0.8 to 0.1 V *vs.* Ag/AgCl over bulk Bi, P-Bi and P-Cu-BiNF. (d) Linearized plot based on the Cottrell equation for bulk Bi, P-Bi and P-Cu-BiNF (The first 250 ms were omitted because of double layer charging effects).

The ECSAs of the catalysts were evaluated according to literature.[1] The chronoamperometric response within 1 s was recorded after applying the potential from 0.8 to 0.1 V (*vs.* Ag/AgCl) in Ar-purged 0.1 M KCl (containing 5 mM $K_3Fe(CN)_6$). ECSA can be obtained by the following Cottrell equation：

$$i = \frac{nFAC\sqrt{D}}{\sqrt{\Pi t}}$$

where i is the current, n = 1, D = 4.34 × 10^{-6} cm^2 s^{-1}, F = 96485 C mol^{-1}, A is ECSA, and C is the concentration of $K_3Fe(CN)_6$ (5 mM).

ECSA can be obtained by plotting *i* versus $t^{-1/2}$ and extracting the slope from the linear part. According to the results, the ECSAs of bulk Bi, P-Bi and P-Cu-BiNF were assessed to be 0.0044, 0.0048 and 0.032 cm^2, respectively. And the ECSAs of P-Cu-BiNF-0.5, P-Cu-BiNF and P-Cu-BiNF-10 with different Cu contents are 0.020, 0.032 and 0.0065 cm^2, respectively.

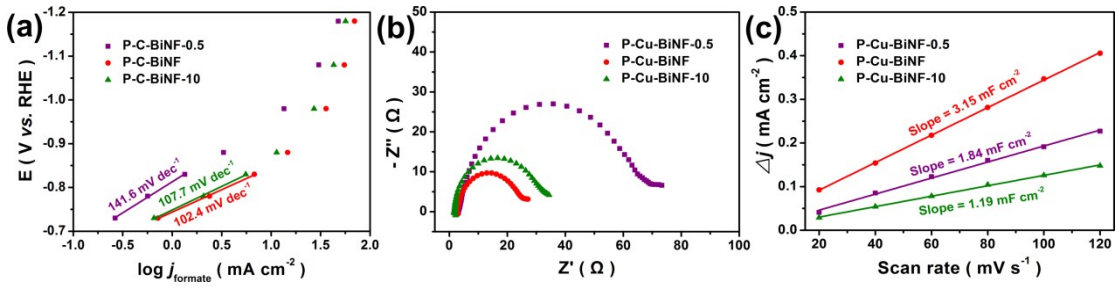

Fig. S16 (a) Tafel plots, (b) electrochemical impedance plots and (c) capacitive Δj (= $j_a - j_c$) against scan rates for P-Cu-BiNF-0.5, P-Cu-BiNF and P-Cu-BiNF-10.

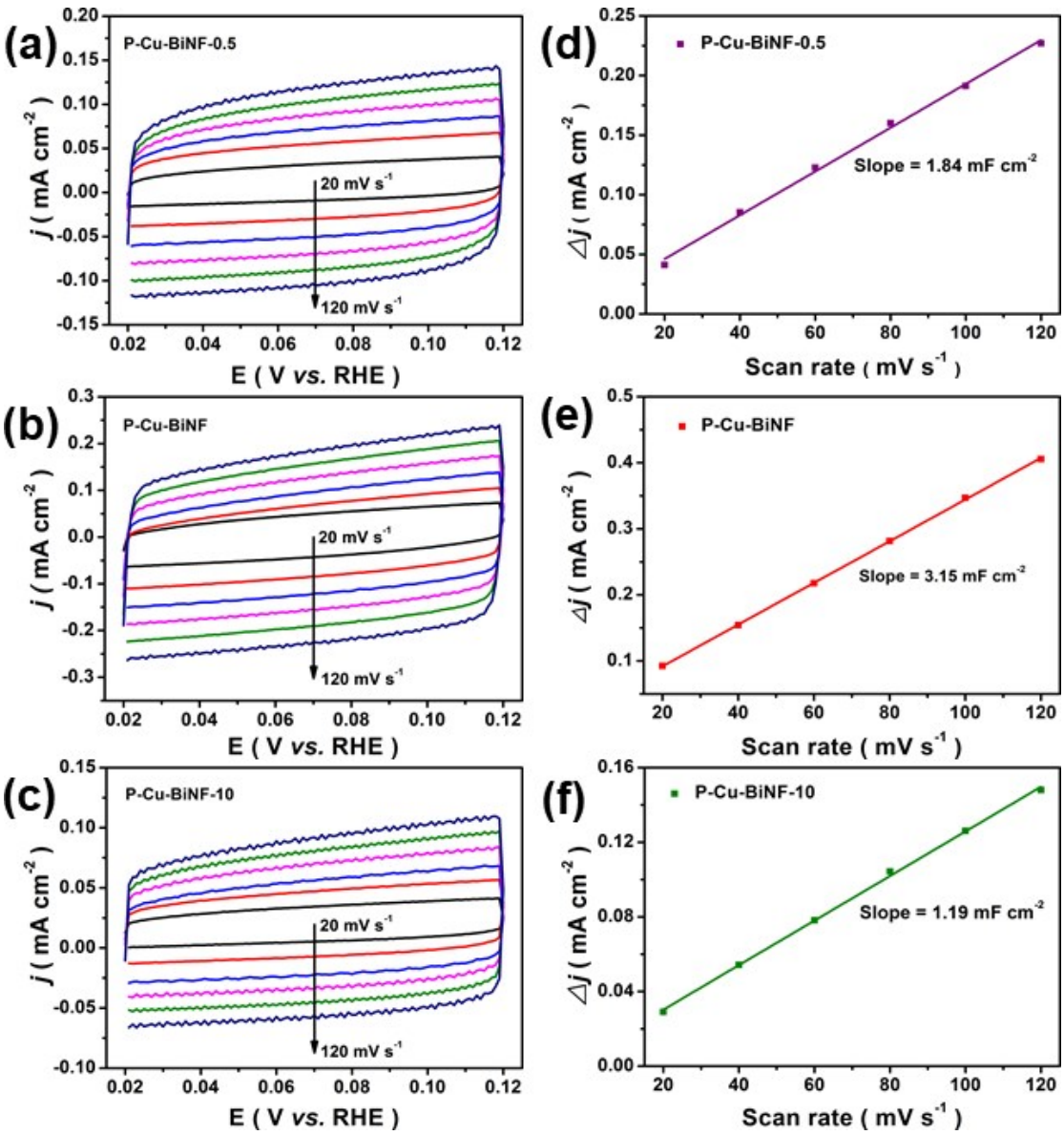

Fig. S17 CV curves at different scan rates and capacitive Δj ($= j_a - j_c$) against scan rates for (a, d) P-Cu-BiNF-0.5, (b, e) P-Cu-BiNF and (c, f) P-Cu-BiNF-10.

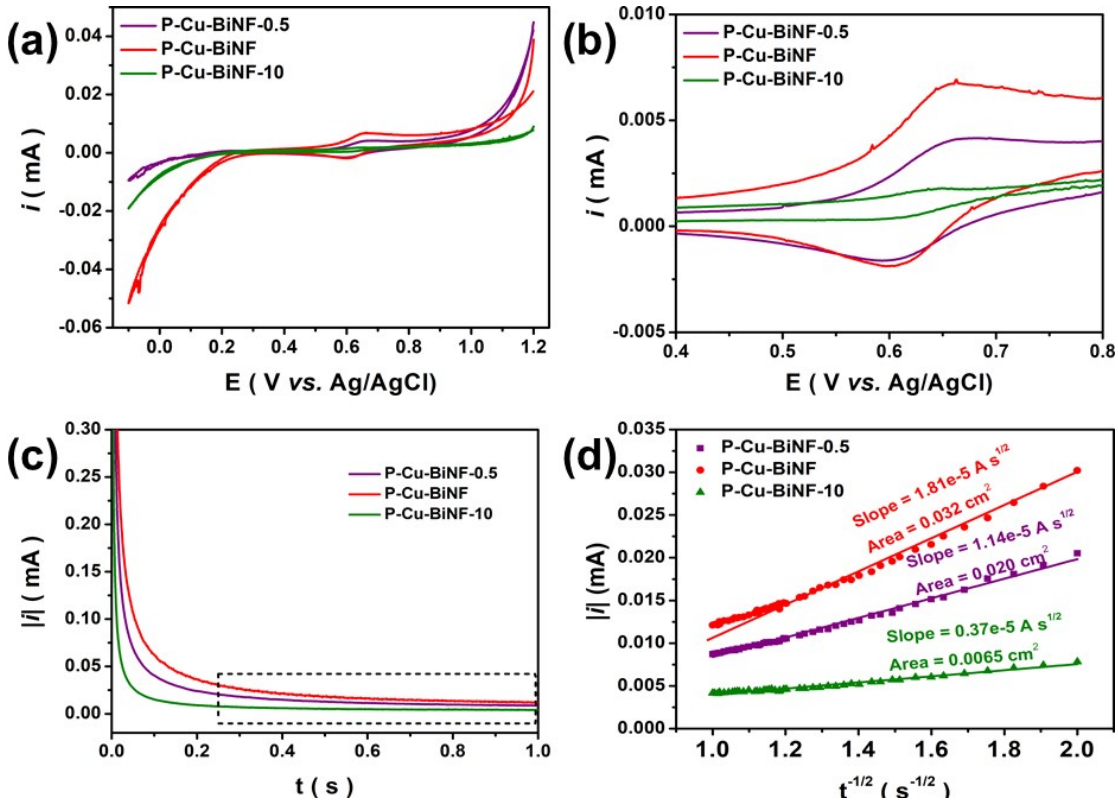

Figure S18 (a) CV curves at the sweep rate of 5 mV s^{-1} in 0.1 M KCl (containing 5 mM $K_3Fe(CN)_6$) over P-Cu-BiNF-0.5, P-Cu-BiNF and P-Cu-BiNF-10. (b) Chronoamperometric response recorded in 0.1 M KCl (containing 5 mM $K_3Fe(CN)_6$) after stepping the potential from 0.8 to 0.1 V *vs.* Ag/AgCl at P-Cu-BiNF-0.5, P-Cu-BiNF and P-Cu-BiNF-10. (c) The magnified of (a). (d) Linearized plot based on the Cottrell equation for P-Cu-BiNF-0.5, P-Cu-BiNF and P-Cu-BiNF-10 (The first 250 ms were omitted because of double layer charging effects).

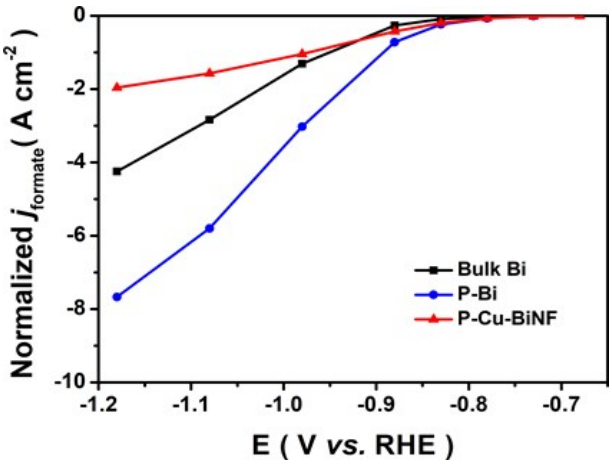

Fig. S19 Formate partial current density normalized by ECSAs of bulk Bi, P-Bi and P-Cu-BiNF.

Table S1 Performance comparison of P-Cu-BiNF with other recently reported Bi-based electrocatalysts for the CO_2-to-formate conversion.

Electrocatalysts	Eletrolyte	Potential (V *vs.* RHE)	$j_{formate}$ (mA cm^{-2})	$FE_{formate}$ (%)	Ref.
P-Cu-BiNF	**0.5 M $KHCO_3$**	**−0.78**	**2.4**	**90.4**	**This work**
		−0.83	**6.8**	**93.3**	
		−0.88	**14.7**	**92.8**	
		−0.98	**36.0**	**92.9**	
		−1.08	**55.0**	**91.5**	
Commercial Bi	0.5 M $KHCO_3$	-0.98	6.3	93.1	
Bismuth oxides	0.5 M $KHCO_3$	-0.9	8	91	2
BOCNS	0.5 M $KHCO_3$	-0.7	9.35	85	3
Bi nanodendrite	0.5 M $KHCO_3$	-0.74	2.4	89	4
Bi nanosheets	0.5 M $KHCO_3$	-1.74 *vs.* SCE	24	>90	5
Bi nanoflower	0.5 M $KHCO_3$	-0.53 *vs*. SCE	7.5	99.2	6
Bi nanoparticle	0.5 M $KHCO_3$	-0.78	~3.3	91.3	7
Bismuth nanoflake	0.1 M $KHCO_3$	-0.6	n.a.[a]	99	8
Bi NPs/Bi_2O_3 NSs with GBs	0.5 M $KHCO_3$	-0.86	6.2	~100	9
Bismuth dendrites on copper mesh	0.5 M $KHCO_3$	-1.26	68.51	~100	10
Bi_2O_3-$CuO_{(x)}$	0.5 M $KHCO_3$	-1.4 *vs*. SCE	9.1	89.3	11
SnO-Bi nanosheet	0.1 M $KHCO_3$	-1.7 *vs.* Ag/AgCl	12	93	12
CuBi	0.5 M $KHCO_3$	-1.5	~60	~90	13
Zn-Bi nanoparticles	0.5 M $KHCO_3$	-0.8	n.a.	94	14
Cu-Bi microspheres	0.5 M $KHCO_3$	-0.93	~6	95	15
Nano-Bi on Copper foil	0.1 M $KHCO_3$	-0.89	2.8	91.3	16

[a] n.a. means no available data.

Note: If the $FE_{formate}$ and $j_{formate}$ values are not specifically stated, they are derived from graphical results or calculated with the available information

References

1. H. Liang, S. Zhao, X. Hu, M. Ceccato, T. Skrydstrup, K. Daasbjery, Hydrophobic Copper Interfaces Boost Electroreduction of Carbon Dioxide to Ethylene in Water, *ACS Catal.*, 2021, **11**, 958-966.
2. P. Deng, H. Wang, R. Qi, J. Zhu, S. Chen, F. Yang, L. Zhou, K. Qi, H. Liu and B. Y. Xia, Bismuth Oxides with Enhanced Bismuth–Oxygen Structure for Efficient Electrochemical Reduction of Carbon Dioxide to Formate, *ACS Catal.*, 2020, **10**, 743-750.
3. Y. Zhang, X. Zhang, Y. Ling, F. Li, A. M. Bond and J. Zhang, Controllable Synthesis of Few-Layer Bismuth Subcarbonate by Electrochemical Exfoliation for Enhanced CO_2 Reduction Performance, *Angew. Chem. Int. Ed.*, 2018, **57**, 13283-13287.
4. J. H. Koh, D. H. Won, T. Eom, N.-K. Kim, K. D. Jung, H. Kim, Y. J. Hwang and B. K. Min, Facile CO_2 Electro-Reduction to Formate via Oxygen Bidentate Intermediate Stabilized by High-Index Planes of Bi Dendrite Catalyst, *ACS Catal.*, 2017, **7**, 5071-5077.
5. N. Han, Y. Wang, H. Yang, J. Deng, J. Wu, Y. Li and Y. Li, Ultrathin bismuth nanosheets from in situ topotactic transformation for selective electrocatalytic CO_2 reduction to formate, *Nat. Commun.*, 2018, **9**, 1320.
6. Y. Qiu, J. Du, C. Dai, W. Dong and C. Tao, Bismuth Nano-Flowers as a Highly Selective Catalyst for Electrochemical Reduction of CO_2 to Formate, *J. Electrochem. Soc.*, 2018, **165**, H594-H600.
7. X. Zhang, X. Hou, Q. Zhang, Y. Cai, Y. Liu and J. Qiao, Polyethylene glycol induced reconstructing Bi nanoparticle size for stabilized CO_2 electroreduction to formate, *J. Catal.*, 2018, **365**, 63-70.
8. S. Kim, W. J. Dong, S. Gim, W. Sohn, J. Y. Park, C. J. Yoo, H. W. Jang and J.-L. Lee, Shape-controlled bismuth nanoflakes as highly selective catalysts for electrochemical carbon dioxide reduction to formate, *Nano Energy*, 2017, **39**, 44-52.
9. L. Li, D.-K. Ma, F. Qi, W. Chen and S. Huang, Bi nanoparticles/Bi_2O_3

nanosheets with abundant grain boundaries for efficient electrocatalytic CO_2 reduction, *Electrochim. Acta*, 2019, **298**, 580-586.

10. C. Zhu, Q. Wang and C. Wu, Rapid and scalable synthesis of bismuth dendrites on copper mesh as a high-performance cathode for electroreduction of CO_2 to formate, *J. CO_2 Util.*, 2020, **36**, 96-104.
11. C. Dai, Y. Qiu, Y. He, Q. Zhang, R. Liu, J. Du and C. Tao, Controlled synthesis of a Bi_2O_3–CuO catalyst for selective electrochemical reduction of CO_2 to formate, *New J. Chem.*, 2019, **43**, 3493-3499.
12. X. An, S. Li, A. Yoshida, T. Yu, Z. Wang, X. Hao, A. Abudula and G. Guan, Bi-Doped SnO Nanosheets Supported on Cu Foam for Electrochemical Reduction of CO_2 to HCOOH, *ACS Appl. Mater. Inter.*, 2019, **11**, 42114-42122.
13. M. Y. Zu, L. Zhang, C. Wang, L. R. Zheng and H. G. Yang, Copper-modulated bismuth nanocrystals alter the formate formation pathway to achieve highly selective CO_2 electroreduction, *J. Mater. Chem. A*, 2018, **6**, 16804-16809.
14. T. Zhang, Y. Qiu, P. Yao, X. Li and H. Zhang, Bi-Modified Zn Catalyst for Efficient CO_2 Electrochemical Reduction to Formate, *ACS Sustain. Chem. Eng.*, 2019, **7**, 15190-15196.
15. L. Jia, H. Yang, J. Deng, J. Chen, Y. Zhou, P. Ding, L. Li, N. Han and Y. Li, Copper-Bismuth Bimetallic Microspheres for Selective Electrocatalytic Reduction of CO_2 to Formate, *Chinese J. Chem.*, 2019, **37**, 497-500.
16. W. Lv, J. Zhou, J. Bei, R. Zhang, L. Wang, Q. Xu and W. Wang, Electrodeposition of nano-sized bismuth on copper foil as electrocatalyst for reduction of CO_2 to formate, *Appl. Surf. Sci.*, 2017, **393**, 191-196.